Shahrood University of Technology

Journal of Mining and Environment (JME)

Journal homepage: www.jme.shahroodut.ac.ir

Iranian Society of Mining Engineering (IRSME)

Sulfate Adsorption Mechanism Investigation from Acid Mine Drainage and Seawater Modification Method on Red Mud: Laboratory Studies and Molecular Simulation

Shima Rahimi, and Mehdi Irannajad

Department of Mining Engineering, Faculty of Mining Engineering, Amir Kabir University of Technology, Tehran, Iran

Article Info

Received 14 May 2025

Received in Revised form 14 May 2025

Accepted 9 June 2025

Published online 9 June 2025

DOI: 10.22044/jme.2025.16215.3137

Keywords

Sulfate

Adsorption

Red mud

Seawater

Molecular simulation

Abstract

In this study, Red Mud (RM) as a byproduct in alumina production process from bauxite was used as an adsorbent for sulfate contaminant adsorption from acid mine drainage (AMD). AMD discharge led to the acidification of water which has detrimental effects on aquatic life and human health. Analytical methods, laboratory studies and molecular simulations were conducted to investigate sulfate adsorption on RM. Thermodynamic calculations were performed after optimizing of existing metal oxide in RM structure with the Material Studio software using the dmol3 and DFT method. The adsorption energy results by Adsorption locator module determined -819.09, -561.7, -268.8, -105.4, and -314.7 kcal/mol for Fe2O3, Al2O3, CaCO3, TiO2 and SiO2, respectively. The most active compounds in RM structure (iron and aluminum oxides) account for 22.5% and 13.3% in the red mud structure, respectively. In addition, seawater washing was employed as RM modification methods, and it could decrease high rates of pH and improve the sorption capacity of raw RM. The effect of this modification was investigated by simulation of solvent in adsorption environment of sulfate on RM and the dielectric constant selection. For water as the primary solvent with a dielectric constant of 78.54, adsorption energy for RM was calculated to be -35.68 kcal/mol and it was increased to -56.69 kcal/mol for the seawater medium with a dielectric constant of 86. Therefore, RM can be considered as a potential sulfate adsorbent because of cost-effectiveness and alkaline pH that can lead to the neutralization of AMD.

1. Introduction

Acid Mine drainage (AMD) is well-known as an important source of surface and underground water pollution all over the world that is produced specially from mining activities [1, 2]. AMD is released when sulfides are exposed to air and water [3]. Also, it often contains elevated levels of sulfate (500-2000 mg/L), and it is also produced from electroplating, steel pickling, nonferrous smelting, and other related materials or substances [4]. The high sulfate content causes low-pH water and sulfuric acid formation. This issue is due to the dissolution of toxic and heavy metals and creates unacceptable levels of these metals in water [5]. The production of AMD results in the death of vegetation and aquatic life, mineralization of water, corrosion of reinforced steel, scaling of equipment, damage to mammals and endangering human health, and corrosion of mine equipment [6].

Nonetheless, several methods have been employed to the treatment of sulfate-containing wastewater, including chemical precipitation, crystallization [7], ion exchange, biological treatment [8], electro-dialysis [9], nano-filtration [10], adsorption and reverse osmosis [11]. Most processes have significant disadvantages such as the need for high energy and costly processes, low efficiency, production of high amounts of sludge, high levels of trace elements, and reclamation processes [5]. Among these processes, adsorption is commonly considered to be the most attractive and used technique due to its low cost, eco-friendliness, and high performance. An adsorbent

Corresponding author: sh.rahimi1983@yahoo.com (sh. Rahimi)

can be assumed as low cost if it requires little processing, abundant in nature, or a by-product or waste material from another industry.

Red mud (RM) is produced as a by-product during the alkaline leaching of bauxite in the Bayer process. According to previous evidence, [12, 13], the production of 1 ton of alumina generally results in the creation of 0.3-2.5 t of RM strongly alkaline (pH = 12-13). High alkalinity, large amounts, and fine-grained nature (90% below the size of 75 μm) of RM cause serious environmental problems [14, 15]. It is also composed of a mixture of solid and metallic oxides. The red color arises from hematite, which can comprise up to 60% of the mass. The red mud is highly basic with a pH ranging from 10 to 13. In addition to iron, the other dominant components include silica, unleached residual aluminum compounds, and titanium oxide [16, 17]. On the other hand, RM is introduced as an unexpansive adsorbent for various contaminants due to its high metal oxide content and activated compound [12, 18]. Further, various methods of surface modification have been implemented to improve the adsorption properties and enhance the adsorption amount of red mud and its pH reduction [19]. These methods include sea water treatment, heat activation, acid washing, and granular with bentonite or fly ash and presence of different surfactants [20]. In this research, aimed to test RM as an alternate sulfate adsorbent and described the results of an investigation on the sulfate removing and seawater effects were studied as a natural, low-cost and available material on red mud treatment.

Molecular simulation methods were applied for microscopic analyses and physical phenomena investigation at molecular level. In these methods, the constituent species of a system such as: molecules and fine particles have been explored. One of the most important software which was applied for modeling, visualization, and analysis of material systems is Materials Studio. This software was utilized in advanced research about various materials such as: polymers, carbon nanotubes, catalysts, and metals. To investigate sulfate ions' adsorption energy and behavior on red mud, we studied a new approach for sulfate adsorption by performing theoretical calculations on metal oxides in the RM structure. It extends beyond the traditional static DFT (density functional theory) calculations, such as molecular quantum simulations, geometry optimization, and vibrational frequency calculations. Remarkably, Materials Studio was used for modelling, visualization, and analysis of material systems as one of the essential software and Fe_2O_3, Al_2O_3, $CaCO_3$, SiO_2, MgO, Na_2O and TiO_2 surfaces were used for these calculations [21, 22]. In addition, calculations were performed to utilize the continuum solvation model, namely COSMO, to simulate modified methods and represent the local environments (water and seawater). Finally, the results of the adsorption energies for sulfate were reported and compared in diverse local environments. The research has expanded the experimentally reported effects such as sulfate removal, adsorption capacity, and computational modelling results.

2. Material and Methods

2.1. Material

RM samples were provided by the Jajarm mine, which produces RM as a by-product during the alkaline leaching of bauxite in the Bayer process. RM was applied as the base material of the adsorbent from this mine that is located 5 km from Jajarm in north Khorasan province of Iran. The X-ray fluorescence (XRF) results and X-ray diffraction (XRD) studies of RM are provided in table 1 and its size distribution is shown in figure 1. Activated RM by seawater was used to improve the reactivity of RM for the removal of sulfate ions in the solution. The sulfate solution was prepared by sodium sulfate (Na_2SO_4), and the solution of ionic strength was adjusted using NaCl (1M). HCl and sodium hydroxide (NaOH) were employed for adjusting the pH of the solution. Also, reagents were used for sulfate concentration measurement in solutions by UV-VIS spectrophotometers such as Glycerol and Isopropyl Alcohol. All reagents were supplied by Merck and were illustrated in table 2.

2.2. RM modification

Employing RM as adsorbent, it was micronized and then sieved through a 100-mesh screen to obtain D_{100} of less than 150 μm. Next RM was suspended in a solution of seawater with a 10% solid percentage for 1 hr (RMS) and mixed for 1 hr to decrease its pH. This can lead to the precipitation of hydroxide, carbonate or hydroxyl carbonate and a decrease in the pH rate to 8-8.5. Then, it was filtered and dried in the oven overnight (100 $^{\circ}$C). Finally, RMS was ground and then sieved through a 75 μm screen [23].

Table 1. Chemical and mineralogical compositions of the red mud.

Chemical composition		Mineralogical composition	
Constituent	**% (w/w)**	**Minerals**	**Formula**
Fe_2O_3	22.5	Calcite	$Ca_{5.23}Mg_{0.77}C_6O_{18}$
Al_2O_3	13.3	Diopside	$Ca_{3.58}Mg_{3.55}K_{0.29}Al_{0.84}Si_{7.74}O_{24}$
SiO_2	15.2	Magnetite	$Fe_{24}O_{32}$
MgO	1.7	Vermiculite	$Si_{5.53}Al_{3.36}Fe_{0.41}Mg_{4.04}Ti_{0.08}O_{30.32}Ca_{0.86}$
K_2O	0.53	Ilmenite	$Fe_6Ti_6O_{18}$
TiO_2	6.7	Katoite	$Ca_{24}Al_{16}Si_{24}O_{96}$
MnO	0.104	Hematite	Fe_2O_3
CaO	18.5	Rutile	TiO_2
P_2O_5	0.14	Sodalite	$Na_2O.Al_2O_{3.1.68}\ SiO_{2.1.73}H_2O$
SO_3	0.47		
LOI	16.6		

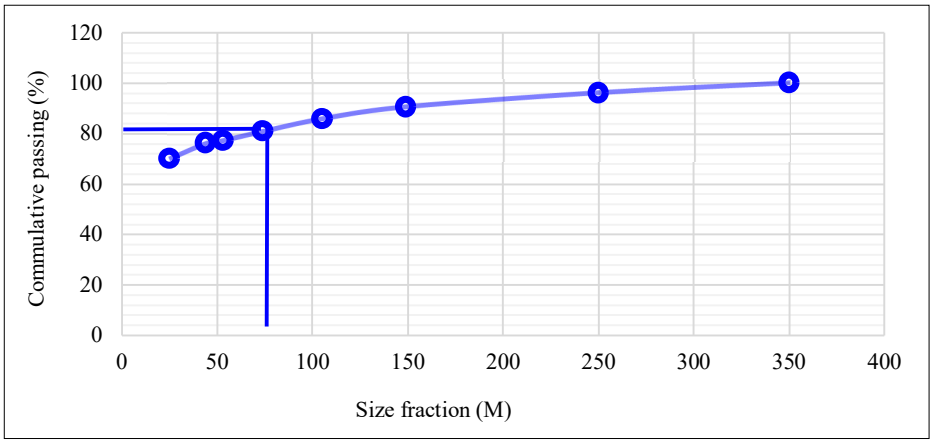

Figure 1. Size distribution plot of RM.

Table 2. Used chemical compositions in adsorption experiments.

Chemical compound name	Formula	Application	Purity (%)	Company
Distilled water	H_2O	Adsorption solution	-	Aryateb
Hydrochloric acid	HCl	Adjusting pH	37	Merk
Sodium hydroxide	NaOH	Adjusting pH	95	Merk
Sea water	-	RM modification	-	-
Sodium chloride	NaCl	Adjusting ionic strength	95	Merk
Glycerol	$C_3H_8O_3$	Sulfate reagent solution	99	Merk
Isopropyl Alcohol	C_3H_8O	Sulfate reagent solution	99	Merk

2.3. Batch adsorption studies

The adsorption experiments were performed using the batch method in a 250 mL Erlenmeyer flask with a constant stirring rate of 420 rpm, at a temperature of 25 ºC, and ionic strength of 0.01 M of NaCl. The sulfate solution with a desired concentration and contact time was prepared and placed in contact with raw and activated RM (0.5-5 g /L) and underwent stirring. Then the sulfate solution was prepared with desired concentrations, followed by placing the raw and activated RM in contact with 100 mL sulfate solution and stirring. After equilibrium, the solution was filtered by Whatman filter paper No. 42 and a clear aliquot of the supernatant was taken accordingly. For sulfate ion measurement, by a UV-VIS spectrophotometer (model HITACHI U-2000), they were prepared standard and specific solution with 5, 10, 15 and 20 ppm sulfate concentration ($Na_2\ SO_4$) for instument calibration. According to previous research, the sulfate percentage in the solution was determined in 420 nm and adding sulfate reagents solution. This solution included Isopropyl Alcohol, Glycerol, Hydrochloric acid and Sodium chloride which was added as identifier befor sulfate content measurment. Ultimately, the sulfate removal (R) and capacity adsorption of the adsorbent (q_e) were calculated using the following equation (1 and 2) [24]:

$$R=\frac{(C_0-C_e)}{C_0}\times 100 \quad (1)$$

$$q_e=\frac{(C_0-C_e)}{M}\times V \quad (2)$$

Where R is the sulfate removal percentage (%), and C_0 is the initial adsorbate concentration (mg/L). Furthermore, C_e and q_e represent the final adsorbate concentration in the solution after equilibrium adsorption (mg/L) and the amount of the adsorbed sulfate per unit of adsorbents (mg/g), respectively. Finally, M is the weight of the adsorbent (g), and V denotes the volume solution (L).

2.4. Equilibrium studies

For equilibrium isotherm investigation, 100 mL of the sulfate solution with various concentrations (250, 500, 750, 1000, 1500, and 2000 ppm) were stirred with 2 g of RM and RMS for 60 min (equilibrium time) at 420 rpm and at pH rate of 6.5-7. The equilibrium isotherms of sulfate adsorption were evaluated by Langmuir, Freundlich, Temkin, and Dubinin -Radushkevich models to study the removal amount of sulfate at equilibrium by the unit mass of the adsorbent from the solution at a constant temperature. Equations, Linear expressions, and parameters related to these models are presented in table 3 [15].

2.5. Kinetic studies

The adsorption kinetics of sulfate onto RM, and RMS was evaluated by pseudo-first-order, pseudo-second-order, Elovich, and intraparticle diffusion kinetic models (table 4) to study the mechanism and rate-controlling step of adsorption. The kinetic model parameters were determined using the least-squares linear regression method. Additionally, the kinetic models of the pseudo-first order and pseudo-second order were investigated to determine the reaction mechanism (chemical or physical). To examine the kinetic isotherms, the sulfate solution with a concentration of 1000 ppm was stirred by 2 g of the adsorbent at 420 rpm and a pH rate of 6.5-7 for different times (10, 20, 30, 60, and 120 min), followed by calculating the parameters and validity of the kinetic models (correlation coefficients).

Table 3. Isotherm models.

Isotherm models	Equations	Linear expression	Parameters
Langmuir	$q_e=q_m\frac{b\,C_e}{1+b\,C_e}$	$\frac{C_e}{q_e}=\frac{1}{q_m}b+\frac{C_e}{q_m}$	qm:(slope) −1, b: slope/intercept
Freundlich	$q_e=K_fC_e^{1/n}$	$\log q_e=\log K_f+\frac{1}{n}\log C_e$	Kf: exp(intercept), n:(slope) −1
Temkin	$q_e=\frac{RT}{B_T\ln A_T}+\frac{RT}{B_T\ln C_e}$	$q_e=\frac{RT}{B_T\ln A_T}+\frac{RT}{B_T\ln C_e}$	BT: RT/slope, AT:exp (intercept BT/RT)
Dubinin–Radushkevich	$q_e=q_m\exp(-\beta\varepsilon^2)$	$\ln q_e=\ln q_m-\beta\varepsilon^2$	qm: exp (intercept), β: - slope $\varepsilon=RT\ln(1+\frac{1}{C_e})$

Table 4. Kinetic models.

Kinetic models	Equations	Linear expression	Parameters
Pseudo-first order	$q_t=q_e[1-\exp(-k_{1p}t)]$	$\ln(q_e-q_t)=\ln q_e-k_{1p}t$	qe=exp(intercept), k1p=−(slope)
Pseudo-second order	$q_t=k_{2p}q_e^2\,t/(1+q_ek_{2p}t)$	$\frac{t}{q_t}=\frac{1}{k_{2p}q_e^2}+t/q_e$	qe=slope−1,k2p=(slope2)/ intercept
Elovich	$q_t=\beta\ln(\beta\alpha t)$	$q_t=\beta\ln(\alpha\beta)+\beta\ln t$	β=slope, α=(slope)−1exp (intercept /slope)
Intraparticle diffusion	$q_t=k_pt^{0.5}$	$\log q_t=\log k_p+0.5\log t$	kp =exp (intercept)

2.6. Thermodynamic studies

To calculate thermodynamic parameters such as Gibbs free energy (ΔG), entropy (ΔS) and enthalpy (ΔH), the 250 ml of sulfate solution with 1000 ppm concentration was prepared and stirred with 2 g/L adsorbent dosage and pH = 7 for 60 min in different temperatures. The stirring incubator was adjusted to temperatures of 298, 303, 313, 323, and 333 K, with the constant stirring rate for ΔG, ΔS, and ΔH calculations (Equation 3, 4 and 5).

$$k_d=\frac{(C_0-C_e)V}{C_eW} \quad (3)$$

$$\ln k_d=\frac{\Delta S^0_{ads}}{R}-\frac{\Delta H^0_{ads}}{RT} \quad (4)$$

$$\Delta G^0_{ads}=\Delta H^0_{ads}-T\,\Delta S^0_{ads} \quad (5)$$

As can be observed in the above Equation, k_d is the distribution coefficient (mg/L) that was calculated in Equation 3 (Where C_0 is initial sulfate

concentration (mg/L), and C_e is final sulfate concentration in the solution after equilibrium adsorption (mg/L). M and V represent the weight of the adsorbent (g), and volume solution (L), respectively. In Equation 4, T denotes solution temperature (K), and R is the universal gas constant (8.314 J/mol k). For thermodynamic parameters calculation, k_d was plotted on a 1/T curve and obtained $\frac{\Delta S^0_{ads}}{R}$ and $\frac{\Delta H^0_{ads}}{R}$ as intercept elevation and slop curve, respectively [24], were calculated according to Equations 4 and 5.

2.7. Molecular simulation

Main oxides were simulated for molecular modeling of sulfate adsorption on RM surface. The main oxides in the RM structure were just considered (chemical composition amount > 5%) to simplify and minimize the calculation cost. Molecular modeling was applied to the adsorption mechanism of sulfate ions on red mud structure. The Dmol3 module was used for DFT calculation in Material Studio software, version 2020. The iron, aluminum, calcium, silicon and titanium oxides were modeled by the generalized gradient functional of BLYP (Becke exchange plus Lee-Yang-Parr correlation). To achieve the best possible accuracy, a double numerical method was applied to all atoms, along with p-function polarization for hydrogen atoms (DNP). The most essential convergence for geometry optimization is summarized in table 5 [25], This work's results were based on "all-electron relativistic" calculation without effective core potentials or pseudo-potentials.

Noteworthy, Fe_2O_3, Al_2O_3, $CaCO_3$, SiO_2, TiO_2, and Na_2O were built as crystal structures for adsorption energy calculation. The desired elements, the number of atoms, and the appropriate lattice parameters for each structure were selected. To investigate the adsorption of sulfate ions on red mud, we used the optimized crystal (with DMol3 module) as the basis of building models for red mud. Afterwards, the cleavage surface was created, and the 2×1 supercells were expanded. Finally, a vacuum slab was built with appropriate thickness for all species of crystals. In table 6, the lattice parameter, the cleavage surface, and the cutoff distance for each structure are illustrated. After that, the optimized sulfate ion was placed near the crystals' surface, and molecular simulations were performed with the DMol3 module. The details of the molecular simulations and our study's results are presented in the results section. The adsorption energy is calculated using Equation 6 [26].

$$E_{adsorption} = E_{surf+adsorbate} - (E_{surf} + E_{adsorbate}) \quad (6)$$

Wherever $E_{adsorption}$ is the adsorption energy, $E_{surf+adsorbate}$ is the total energy of the surface with the adsorbed molecule, E_{surf} is the total energy of the clean surface, and $E_{adsorbate}$ is the total energy of the isolated adsorbate molecule.

As mentioned above, seawater washing was used in the experimental section for RM surface modification and improving adsorption. To simulate the modification methods and represent the local environment (water, and seawater), calculations were performed utilizing the continuum solvation model, namely COSMO (conductor-like screening model). The dielectric constants of the two solutions are composed of water, and seawater which were considered 78.54, and 84 respectively. The multipolar expansion was used to calculate the solvation energy for the whole model. The geometry optimization was validated based on the vibrational frequency analysis [25].

3. Results and Discussion

3.1. Effect of seawater modification method

The effect of RM dosage on sulfate removal from the aqueous solution at the pH of 6.5-7 is illustrated in figure 2. As shown, sulfate removal efficiency increases by increasing the RM dosage due to increasing the available surface of the adsorbent [21]. As can be seen, the maximum sulfate removal was 6.3, and 29.4% for RM, and RMS in 5 g/L adsorbent dosage. While sorption capacity almost decreases with increasing adsorbent dosage this can be due to a reduction in the number of sulfate ions in the solution compared to adsorbent sites and the maximum sorption capacity is obtained at 15.4 and 3.1 mg/g in 0.5, 2 and 4 g/L adsorbent dosage for RMS and RM, respectively. Further, figure 2 confirms that seawater washing rises sulfate adsorption onto the RM surface.

Table 5. Convergence tolerances for geometry optimization calculations.

Convergence tolerance parameters	
Energy	1×10^{-5} Hartree
Maximum force	2×10^{-3}Hartree/Å
Maximum displacement	5×10^{-3}Hartree
Maximum iterations	50
SCF tolerance	10^{-6} Hartree (fine)
Orbital cut-off	4.6 Å
Core treatment	All electron relativistic
Basis set	DNP
Basis File	4.4

Table 6. Lattice parameter, cleavage surface and cutoff distance of mineral structures.

Mineral name	Crystal system	Space group	Lattice constant	Cleave surface	Cutoff distance (Å)
Hematite	Hexagonal	R3_C	a=5.04, b=5.04, c=13.75, α=90, β=90 and γ=120	0 0 1	12.2
Corundum	Trigonal	R3_C	a=4.75, b=4.75, c=12.98, α=90, β=90 and γ=120	0 0 1	8.4
Calcite	Trigonal	R3_C	a=4.99, b=4.99, c=17.061, α=90, β=90 and γ=120	1 0 1	5.5
α-quartz	Trigonal	p3_221	a=4.91, b=5.405, c=4.916, α=90, β=90 and γ=120	0 1 1	12.5
Rutile	Tetragonal	p4_2/MNM	a=4.592, b=4.592, c=2.957, α=90, β=90 and γ=90	0 1 1	12.5

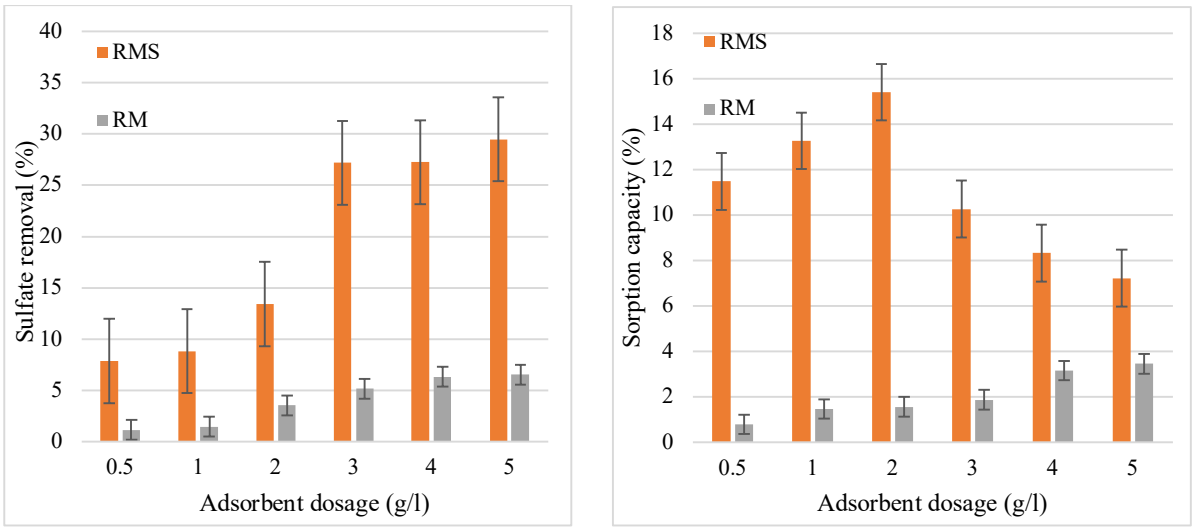

(a) (b)

Figure 2. Effect of adsorbent dosage on sulfate removal (a) and sorption capacity (b) by RM, and RMS (contact time of 60 min, sulfate concentration of 1000 ppm and temperature of 27 ˚C).

3.2. Adsorption isotherm and kinetic models

The data obtained from equilibrium tests was modeled using the linear regression method of least squares and correlation coefficient (R^2). The isotherm model parameters were determined by the solver add-in function in Microsoft Excel. Linear expressions, parameters and R^2 related to each model are listed in table 7.

According to the results of isotherm studies for RM, the order of the best model based on the R^2 values is Freundlich> Dubinin– Radushkevich> Temkin> Langmuir. For RMS, the matching of the sorption isotherm is almost the same as RM; the difference is that the matching of Langmuir is more than the Temkin model. There is more matching with the Freundlich model for RM and RMS with R^2 values 0.97 and 0.94. According to Freundlich isotherm results, maximum sorption capacity for RM and RMS are obtained at 0.88 and 2.45 mg/g. The Freundlich model indicates that the adsorbent surfaces are heterogeneous and the adsorption onto the adsorbent surface is multilayer. Moreover, adsorption is reversible. In this model, the

favorable range of adsorption intensity (n) is $0 < 1/n < 1$, thus adsorption is desirable down. The Dubinin-Radushkevich model investigates maximum sorption capacity that indicates 1.37 and 26.3 for RM and RMS. Also, this model determines the energy of adsorption and type of the adsorption process (physical adsorption ($E < 8$), chemical adsorption or ion exchange ($E > 16$), and particle diffusion that governs the reaction ($E > 16$)). Based on this model, the adsorption process occurs with particle diffusion. In this model, it is assumed that the adsorbed amount for any adsorbate concentrations follows a Gaussian function of the Polanyi potential. The Temkin model evaluates the heat of adsorption and some indirect interactions of the adsorbate/adsorbate in the adsorption process. The increase of B_T for RMS rather than RM indicates that the seawater washing can improve the adsorption process of sulfate on the RM surface [27]. In comparison to the other research for investigation of adsorption isotherm of RM, the most consistent was with Freundlich isotherm [28].

The adsorption kinetics of sulfate on RM, and RMS were evaluated by pseudo-first-order, pseudo-second-order, Elovich, and Intraparticle diffusion kinetic models (Table 8) to examine the mechanism and rate-controlling step of adsorption. The R^2 values (0.95 and 0.84 for RM, and RMS) demonstrated that the pseudo-second-order model outperformed the other kinetic models for the description of sulfate adsorption onto both RMS and RM. These results confirmed that the rate-controlling step in the sulfate adsorption process onto RM and RMS was a chemisorption interaction. According to this model, two reactions (series or in parallel) are proposed, including the fast reaction that quickly reaches equilibrium and the slow reaction that can continue for a long period [29]. The kinetics constants (K) of both pseudo-second order and intraparticle diffusion models are more for RMS compared to RM, indicating a further absorption rate of sulfate onto the RMS surface. The contact time for adsorption equilibrium for other applied adsorbents in sulfate adsorption was 60-120 min, so obtained results for kinetic investigation is in good agreement with other results [30].

Table 7. Isotherm model parameters for sulfate adsorption onto RM and RMS.

Isotherm Models	Parameters	RM	RMS
Langmuir	Linear expression	Y= -1.135X+755.57	Y= -0.4069X+414.6
	q_m	0.88	2.45
	b	-0.001	-0.005
	R^2	0.62	0.57
Freundlich	Linear expression	Y=2.3411X-5.6369	Y= 2.9026X-7.1636
	K_f	2.29×10^{-6}	6.68×10^{-8}
	N	2.34	2.9
	R^2	0.97	0.94
Temkin	Linear expression	Y= 5.4182X-26.981	Y=3.576X-5.5014
	B_T	468.2	709.4
	A_T	0.006	0.21
	R^2	0.69	0.32
Dubinin-Radushkevich	Linear expression	Y= -21.822X+76.301	Y= -0.0378X+3.27
	q_m	1.37	26.3
	β	21.8	0.03
	R^2	0.84	0.84

3.3. Thermodynamic properties

The simulation of single clusters in the RM structure include: Fe_2O_3, Al_2O_3, $CaCO_3$, SiO_2, and TiO_2 were conducted in water environment. DFT was applied for geometry optimization of these structures in the underground state. Figure 3. shows the optimized structure of these clusters and their bond lengths and bond angles. Furthermore, the main thermodynamic properties were calculated for various structures in RM reaction with sulfate ion. The results of a vibrational analysis calculation were used to compute important thermodynamic properties such as enthalpy (H), entropy (S), free energy (G), total energy (E) and heat capacity at constant pressure (Cp) as a function of temperature. DMol3 can be applied as a tool for the prediction of these thermodynamic properties of molecular systems and total energy yields. In this section, the thermodynamic properties of the main chemical composition of RM were calculated in separate documents. Table 9 indicates the calculation results of thermodynamic properties. In figure 4, the results of computed free energy in molecular simulation and obtained free energy from thermodynamic measurements were compared. Results indicated that there is a systematic conformity between the calculated free energy in molecular simulation and obtained free energy from thermodynamic measurements.

Table 8. Kinetic model parameters for sulfate adsorption onto RM and RMS.

Isotherm Models	Parameters	BRM	RMH
Pseudo-first order	Linear expression	Y= 0.0087X+1.8443	Y= 0.0106X+2.046
	q_e	6.32	7.73
	K_1	0.008	0.01
	R^2	0.51	0.42
Pseudo-second order	Linear expression	Y= 0.0545X+1.3812	Y=0.0377X+1.2337
	q_e	18.34	26.52
	K_2	0.19	0.17
	R^2	0.95	0.84
Elovich	Linear expression	Y= 4.3641X-4.3701	Y= 6.8858X- 9.9079
	α	0.33	0.23
	β	0.22	0.14
	R^2	0.79	0.81
Intraparticle diffusion	Linear expression	Y= 1.6056X	Y=0.2365X
	Kp	1.6	0.23
	R^2	0.62	0.63

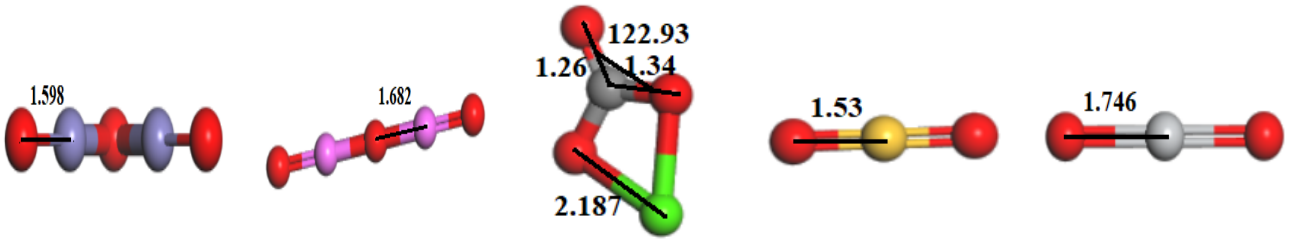

Fe_2O_3 **Al_2O_3** **$CaCO_3$** **SiO_2** **TiO_2**

Figure 3. Optimized structure of clusters and their bond lengths and angles.

Table 9. Calculated thermodynamic properties of reactants and products.

Composition name	S (Cal/mol k)	Cp (Cal/mol k)	H (kcal/mol)	G (kcal/mol)
Al_2O_3	71.485	19.932	10.818	-10.495
Fe_2O_3	77.396	16.756	8.84	-14.236
$CaCO_3$	72.529	16.287	12.878	-8.746
SiO_2	57.433	11.066	6.725	-10.399
TiO_2	55.549	8.277	4.444	55.549
MgO	51.12	7.75	3.167	-12.075

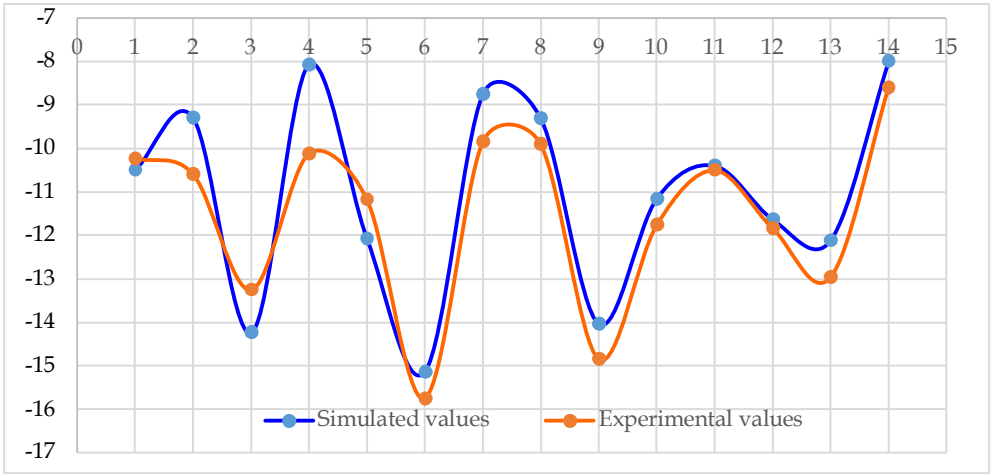

Figure 4. Results of simulated free energy and obtained from thermodynamic measurements. (1:Al_2O_3, 2: Fe_2O_3, 3:$CaCO_3$, 4:SiO_2, 5: TiO_2, 6: MgO, 7: $Al_2(SO_4)_3$, 8:$Fe_2(SO_4)$, 9: $CaSO_4$, 10:Si SO_4, 11: $TiOSO_4$, 12: $MgSO_4$, 13: Na_2O, 14: Na_2SO_4).

3.4. Adsorption energy calculation

In the next step, after optimization of crystal oxide components existed in RM structure, $E_{surf+adsorbate}$, E_{surf} and $E_{adsorbate}$ were calculated for sulfate adsorption energy calculation. The optimized crystal components in RM structure after sulfate ion adsorption on their surface were demonstrated in figure 5. Adsorption bond lengths for each component were measured. The results illustrated that the shortest bond lengths which belonged to Fe_2O_3, Al_2O_3, TiO_2, $CaCO_3$ and SiO_2 and equal to 2.134, 2.745, 2.949, 3.194 and 18.229 Å, respectively. Therefore, the lowest bond length is related to Fe_2O_3, Al_2O_3 and TiO_2 that are main metal oxides and exist in RM structure. The results of adsorption energy calculation in water environment with dielectric constant =78.54 were brought in table 10. The results illustrated that all adsorption energies were negative. This issue showed that all main crystal components in RM structure had a great tendency to adsorption of sulfate ions. Among these crystal oxides, the highest adsorption energy belongs to Fe_2O_3, TiO_2, Al_2O_3, $CaCO_3$ and SiO_2, respectively. Whereas these compounds were the main oxides in RM structure, adsorption energy of RM was negative, too. The calculated adsorption energy for RM was equal to -35.68 kcal/mol.

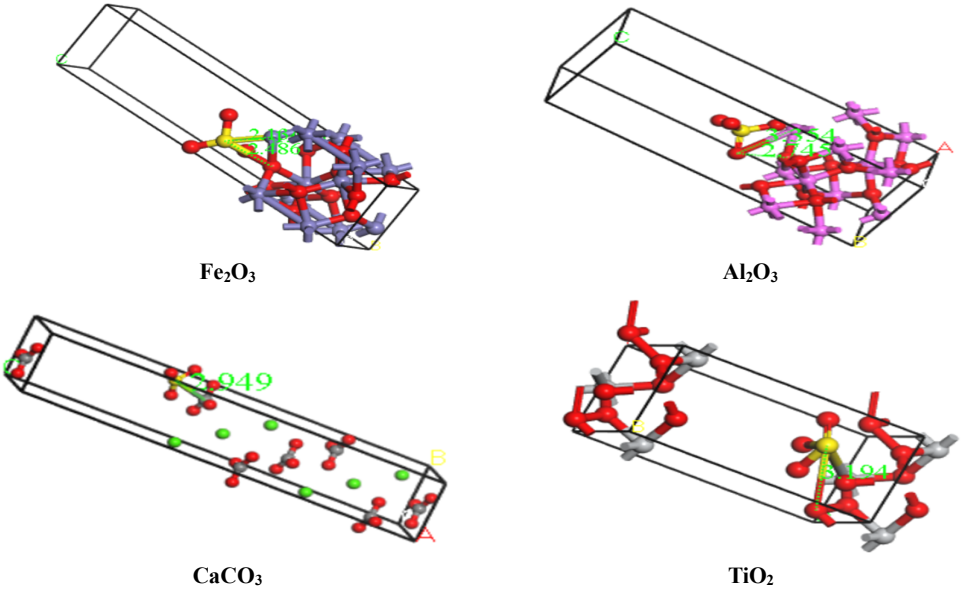

Fe_2O_3 Al_2O_3

$CaCO_3$ TiO_2

Figure 5. Optimized crystal components in RM structure after sulfate ion adsorption.

Table 10. Results of adsorption energy in water environment for different crystal oxide.

Mineral name	E surface or adsorbate	E SO_4^{2-} or adsorbent	E SO_4^{2-}/Surface or adsorbent/adsorbate	E Adsorption (Ha)	E Adsorption (kcal/mol)
Hematite	-8304.7	-700.69	-9008.22	-2.79	-64.33
Quartz	-2136.6	-700.69	-2837.97	-0.63	-14.52
Rutile	-5796.6	-700.69	-6497.7	-0.95	-21.9
Calcite	-5115.5	-700.69	-5817.4	-1.23	-28.36
Corundum	-2254.7	-700.69	-2956.8	-1.43	-32.97

There are various treatment methods for improving adsorption amount and surface modification of RM such as: seawater treatment, acid washing with different acids, heat activation, granular with bentonite or fly ash and presence of different surfactants [21]. In this research, seawater treatment washing was applied for this aim. To simulate this environment (seawater) as solvent, calculations were performed using the continuum solvation model, namely COSMO. All simulation steps for main crystal oxides were repeated in seawater environment with 84 dielectric constants. The results are related to the calculations of simulation in seawater which has been brought in table 11. These results show that with increasing of dielectric constant, adsorption energies for all main crystal oxides existing in RM structure are raising. The adsorption energy for RM structures in seawater environment was equal to -56.69 kcal/mol. These results illustrate that applied

modification method could improve the adsorption properties of raw RM. It is energetically favorable to transfer an ion from the liquid crystal layer with a lower dielectric constant to the alignment layer with a higher dielectric constant. So, with increasing the dielectric constant in adsorption environment, it increases activated sites on surface layer of adsorbent. To increase ion adsorption on the alignment layer, an alignment layer with a higher dielectric constant is helpful. In the case of inorganic material (metal oxides), this issue is helpful in increasing ion adsorption on the alignment layer.

Table 11. Results of adsorption energy in seawater environment for different crystal oxide.z

Mineral name	E surface or adsorbate	E SO_4^{2-} or adsorbent	E SO_4^{2-}/Surface or adsorbent/adsorbate	E Adsorption (Ha)	E Adsorption (kcal/mol)
Hematite	-8304.48	-700.58	-9009.15	-4.09	-94.31
Quartz	-2136.35	-700.58	-2838.05	-1.12	-25.82
Rutile	-5796.23	-700.58	-6498.75	-1.94	-44.73
Calcite	-5115.42	-700.58	-5817.67	-1.23	-38.51
Corundum	-2254.25	-700.58	-2957.47	-2.64	-60.87

3.5. FTIR analysis

The FTIR spectra of RM, and SRM after sulfate adsorption are plotted in figure 6. The bands which appear at 1410-1470 cm^{-1} for adsorbents are related to carbonate bands. Besides, the peak at 1431 cm^{-1} and 1625 cm^{-1} for RM samples corresponds to C-O and C-C stretching vibration that could be attributed to the existence of cancrinite or calcite in RM structure [15]. In addition, the bands in the region of 460-590 and 680 cm^{-1} are the result of the stretching vibrations of the Fe-O bond that can be associated with hematite and magnetite as main composition of RM. Additionally, the bands at around 995 cm^{-1} may correspond to the Si-O-Si and Si-O-Al vibrations that could belong to alumina, Zhypsyt and Boehmite in RM [31]. The peak intensity of calcite (1431 cm^{-1}) in SRM spectra becomes sharper rather than other adsorbents and peak which can be related to OH^- (3420 cm^{-1}) reduction due to the neutralized OH^- ion with Mg, Al and Ca in seawater. As can be seen, there is a sharp intensity absorption around 1100 cm^{-1} that is related to SO_4^{2-} vibration band in RM, and SRM after sulfate adsorption. The intensity of this peak is sharper for SRM than RM, this issue shows more adsorption of sulfate on SRM.

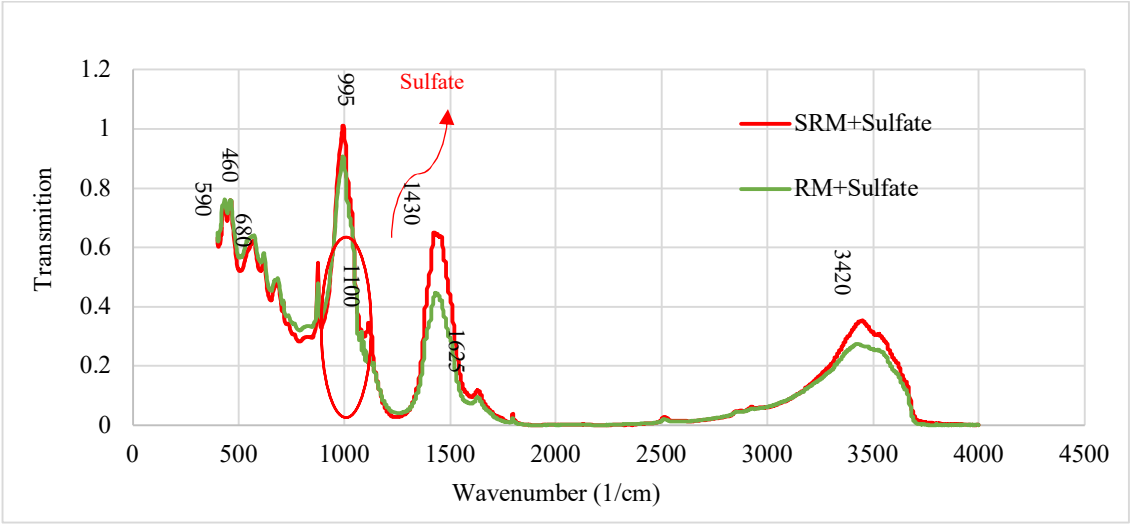

Figure 6. The FTIR spectra of RM, and SRM after sulfate adsorption.

3.6. BET analyses

The specific surface area is an effective factor in the adsorption number of adsorbents. Furthermore, the porosity volume per adsorbent mass indicates its specific surface area. For porosity analysis of RM samples, the nitrogen gas absorption and desorption in a range of relative pressure by a pore analysis device was profoundly investigated. Considerably, this device provides nitrogen gas absorption and desorption isotherm along with the dimensional distribution diagram of pores for samples. Moreover, it provides a

summary for pore analysis report of samples, which includes information about specific surface area, surface area of micropores, total pore volume, pore volume of micropores and average pore diameter. The textural properties of RM and its modified shape are presented in table 12. According to the obtained results, the porosity volume of RMS is 0.034 cm^3/g that has decreased relative to raw RM (0.0686 cm^3/g). The reason may be the precipitation of various salts on the RMS surface from seawater. It can be the result of the existence of a positive layer on RMS surface and the precipitation of various salts on surface from seawater [32].

Table 12. Textural properties of RM and modified RM

Adsorbent	Specific Surface Area (m^2/g)	Dotted Special Surface (m^2/g)	Size Particle (nm)	Volume Porosity (cm^3/g)
RM	28.7	26.5	78.6	0.0686
RMS	12.5	11.9	588.6	0.0345

3.7. SEM and EDX results

Scanning electron microscopic pictures related to RM, and RMS are shown in figure 7. in a, and b sections, respectively. There are particles of various sizes and amorphous or crystalline structures. Metal oxide and primitive minerals, especially iron have crystalline structures and large sizes and amorph minerals that were formed during the Bayer process including sodium and aluminum minerals are smaller. EDX results in figure 8 illustrate the attendance of iron, calcium, titanium and silicon as main constituent elements in RM, and RMS structures. Comparing the EDX result of RMS with RM shows increasing calcium ions in RMS composition due to calcite and aragonite precipitation during seawater treatment.

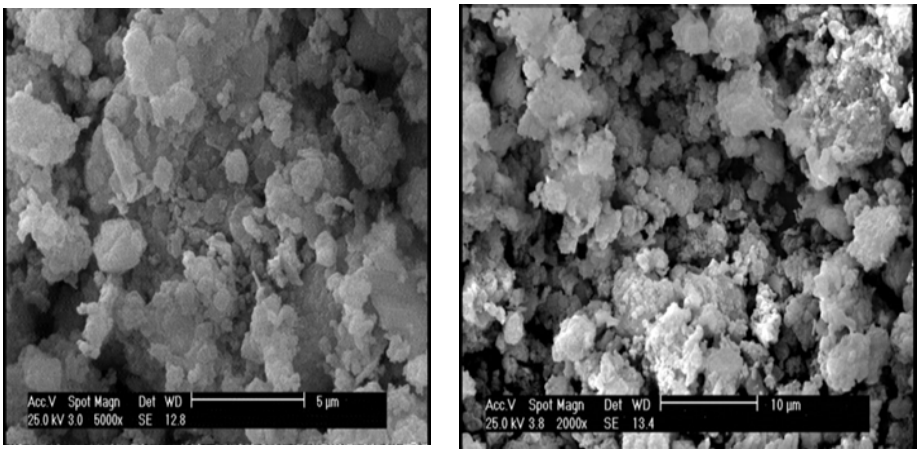

(a) (b)

Figure 7. Scanning electron microscopic of RM (a) and RMS (b).

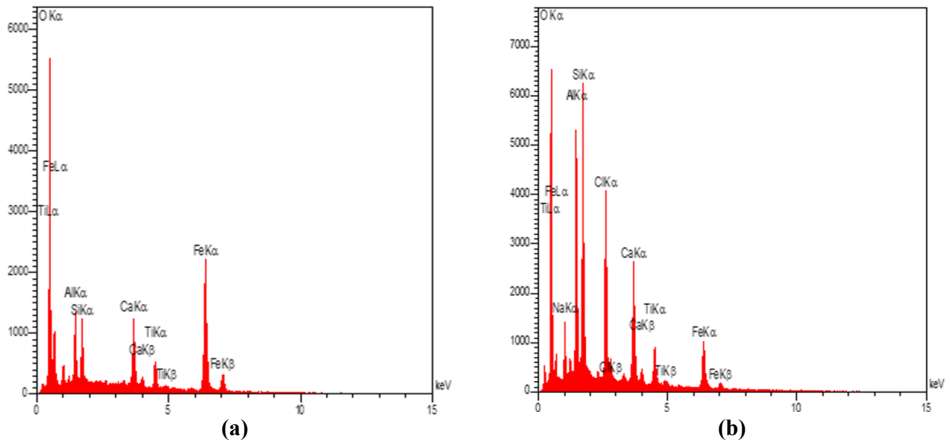

(a) (b)

Figure 8. Energy dispersive X-ray of RM (a) and RMS (b).

4. Conclusions

RM can introduce as an unexpansive adsorbent for sulfate removal from AMD due to its high metal oxides content and high level of pH that can increases low pH of this drainage. Experimental adsorption results illustrate that RM and its activated type by seawater can remove sulfate ions from AMD and sorption capacity by SRM was obtained 15.4 mg/g. Negative adsorption energies for main crystal components in RM structure shows that they have great tendency to sulfate adsorption. Among these crystal oxides, the highest adsorption energy belonged to Fe_2O_3, TiO_2, Al_2O_3, $CaCO_3$ and SiO_2, respectively. Also, seawater treatment as a modification method was used for reducing pH and increasing adsorption capacity of RM. Seawater washing raises sulfate removal from 6.3% for RM to 29.4% for SRM. The adsorption energies for RM structure in water, and seawater using COSMO were calculated -35.68, and -56.69 kcal/mol. These results illustrate that applied modification methods can improve the adsorption properties of raw RM. Comparing the EDX results show increasing calcium ions in RMS composition due to calcite and aragonite precipitation during seawater treatment. Also, there is a sharper intensity absorption related to SO_4^{2-} vibration band in FTIR analyses for SRM than RM after sulfate adsorption. Although RM and its activated type do not have high adsorption capacity and sulfate removal percentages, applying new activation methods include heating and combination with bio absorbent can increase adsorption amount and reduce destructive environmental effects of both RM and AMD. Regeneration study revealed the high reusability (>90%) and acceptable stability of RM even after five successive cycles. These findings indicate that RM use for pollutants removal from wastewater offers a green and environmentally sustainable approach. Although DFT and COSMO models are valuable tools for understanding the thermodynamics of sulfate adsorption, their lack of consideration for kinetics is a limitation.

Acknowledgments

The authors express their deep gratitude to the Amirkabir university and Opal Parsian Sangan Industrial and Mining (OPSIM) for bearing research costs and facilities.

References

[1]. Sinh, P., Yadav, A.K., Pal, Mishra, V. (2020). Water Pollutants: Origin and Status. *Sensors in Water Pollutants Monitoring: Role of Material*: 5–20.

[2]. Manisalidis, I., Stavropoulou, E., Stavropoulos, A., Bezirtzoglou, E. (2020). Environmental and Health Impacts of Air Pollution: A Review. *Front Public Health*, volume 8.

[3]. Alimohammadi, V., Sedighi, M., Jabbari, E. (2017). Optimization of sulfate removal from wastewater using magnetic multi-walled carbon nanotubes by response surface methodology. *Water Sci Technol*, 76:(10) 2593–2602.

[4]. Kitadai, N., Nishiuchi, K., Tanaka, M. (2018). A comprehensive predictive model for sulfate adsorption on oxide minerals. *Geochimica et Cosmochimica Acta*, 238(1): 150-168.

[5]. Halajnia, A., Oustan, S., Najafi, N., Lakzian, A.R. A. (2013). Adsorption–desorption characteristics of nitrate, phosphate and sulfate on Mg–Al layered double hydroxide. *Applied Clay Science*, 80(1): 305-312.

[6]. Baldwin, D. S., and Mitchell, A. (2012). Impact of sulfate pollution on anaerobic biogeochemical cycles in a wetland sediment. *Water research*, 46(4): 965-974.

[7]. Silva, A. M., Lima, R., Leão, V. (2012). Mine water treatment with limestone for sulfate removal. *Journal of hazardous materials*, 221(1): 45-55.

[8]. Liang, F., Xiao, Y., Zhao, F. (2013). Effect of pH on sulfate removal from wastewater using a bioelectrochemical system. *Chemical engineering journal*, 218(1): 147-153.

[9]. Lee, H. J., Oh, S. J., moon, S. H. (2003). Recovery of ammonium sulfate from fermentation waste by electrodialysis, *Water Research*, 37(5): 1091-1099.

[10]. Galiana-Aleixandre, M. V., Iborra-Clar, A., Bes-Pifi, A., Mendoza-Roca, J. A., Cuartas-Uribe, B., IborraClar, M. I. (2005). Nanofiltration for sulfate removal and water reuse of the pickling and tanning processes in a tannery, *Desalination,* 179(1-3): 307-313.

[11]. Bodalo, A., Gomez, J. L., Gomez, E., Leon, G., Tejera, M. (2004). Reduction of sulphate content in aqueous solutions by reverse osmosis using cellulose acetate membranes, *Desalination,* 162(10): 55-60.

[12]. He, J., Jie, Y., Zhang, J., Yu, Y., Zhang, G. (2013). Synthesis and characterization of red mud and rice husk ash-based geopolymer composites, *Cement & Concrete Composites*, 37: 108-118.

[13]. Liu, Y., Naidu, R., Ming, H. (2011). Red mud as an amendment for pollutants in solid and liquid phases, *Geoderma*, 163(1-2): 1-12. https://doi.org/10.1016/j.geoderma.2011.04.002.

[14]. Zhao, Y., Yue, Q., Li, Q., Xu, X., Yang, Z., Wang, X., Gao, B., Yu, H. (2012). Characterization of red mud granular adsorbent (RMGA) and its performance on phosphate removal from aqueous solution, *Chemical Engineering Journal*, 193: 161-168.

[15]. Ye, J., Cong, X., Zhang, P., Zeng, G., Hoffmann, E., Wu, Y., Zhang, H., Fang, W. (2016). Operational parameter impact and back propagation artificial neural network modeling for phosphate adsorption onto acid-activated neutralized red mud, *Journal of Molecular Liquids*, 216(2): 35-41.

[16]. Sutar, H., Mishra, S.Ch., Sahoo, S., and Chakraverty, A. P. (2014). Progress of Red Mud Utilization: An Overview. *American Chemical Science Journal*, 4(3): 255–279.

[17]. Burke, I.T., Peacock, C.L., Lockwood, C.L., Stewart, D.I., Mortimer, R.J.G., Ward, M.B., Renforth, P., Gruiz, K., Mayes, W.M. (2013). Behavior of Aluminum, Arsenic, and Vanadium during the Neutralization of Red Mud Leachate by HCl, Gypsum, or Seawater, *Environmental Science Technology*, 47(12): 6527–6535.

[18]. Palmer, S. J., Nothling, M., Bakon, K. H., Frost, R. L. (2010). Thermally activated seawater neutralized red mud used for the removal of arsenate, vanadate and molybdate from aqueous solutions, *Journal of Colloid and Interface Science*, 342(1): 147–154.

[19]. Schwarz, S., Schwarz, D., Ohmann, W., Neuber, S. (2018). Adsorption and desorption studies on reusing chitosan as an efficient adsorbent. Proceedings of the 3rd World Congress on Civil. *Structural and Environmental Engineering*, 8 – 10.

[20]. Martins, Y. J. C., Almeida, A. C. M., Viegas, B. M., Nascimento, R. A., Ribeiro, N. F. (2020). Use of red mud from amazon region as an adsorbent for the removal of methylene blue: process optimization, isotherm and kinetic studies. *International Journal of Environmental Science and Technology,* 17: 4133–4148.

[21]. Rahimi, Sh., & Irannajad, M. (2024). Sulfate Removal from Acid Mine Drainage with Chitosan-Modified Red Mud Using Analytical Methods: Isotherm, Kinetic, and Thermodynamic Studies. *Journal of Environmental Engineering*, 150(10): 04024041-5.

[22]. Irannajad, M., & Rahimi, Sh. (2024). Density Functional Theory Study of Adsorption Mechanism of Sulfate Contaminant on Red Mud Surfaces, *Environmental engineering science*, 32(5): 240416. http://dx.doi.org/10.1089/ees.2024.0077.

[23]. Rahimi, Sh., & Irannajad, M. (2024). The molecular simulation of sulfate adsorption on hematite and other red mud clusters: Kinetic and thermodynamic modelling study. *Environmental engineering research*, 30(3): 240418. http://dx.doi.org/10.1061/JOEEDU.EEENG-7304.

[24]. Irannajad, M., & Rahimi, Sh. (2024). Sulfate Adsorption Process from Acid Mine Drainage by Seawater and Acid-Activated Neutralized Red Mud. *Chemistry Africa*, 45: 1-10.

[25]. Zia, Y., Mohammadnejad, S., Abdollahy, M. (2019). Gold passivation by sulfur species: A molecular picture, *Minerals Engineering*, 134(6): 215-221.

[26]. Wang, R. B., & Hellman, A. (2018). Initial water adsorption on hematite (α-Fe2O3) (0001): A DFT + U study. *The journal of chemical physics*, 148: 094705-1. https://doi.org/10.1063/1.5020358.

[27]. Li, D., Ding, Y., Li, L., Chang, Z., Rao, Z., Lu, L. (2015). Removal of hexavalent chromium by using red mud activated with cetyl trimethylammonium bromide. *Environmental technology*, 36(9-12): 1084-1090. https://doi.org/10.1080/09593330.2014.975286.

[28]. Deihimi, N., Irannajad, M., Rezai, B. (2019). Removal of ferricyanide ions from aqueous solutions using modified red mud with cetyl trimethylammonium bromide. *Environmental earth sciences*. 78(6): 187-205. https://doi.org/10.1007/s12665-019-8173-8.

[29]. Deihimi, N., Irannajad, M., Rezai, B. (2018). Equilibrium and kinetic studies of ferricyanide adsorption from aqueous solution by activated red mud, *Journal of Environmental Management*. 227(1): 277–285.

[30]. Sadeghalvad, B., Khorshidi, N., Azadmehr, A., Sillanpa, M. (2011). Sorption, mechanism, and behavior of sulfate on various adsorbents: A critical review. *Chemosphere,* 263, 128064.

[31]. Deihimi, N., Irannajad, M., Rezai, B. (2018). Characterization studies of red mud modification processes as adsorbent for enhancing ferricyanide removal, *Journal of Environmental Management*, 206(1): 266-275.

[32]. Moldoveanu, G.A., Papangelakis, V.G. (2012). Recovery of rare earth elements adsorbed on clay minerals: I. Desorption mechanism. *Hydrometallurgy,* 117(1): 71 – 7.

انجمن مهندسی معدن ایران
نشریه مهندسی معدن و محیط زیست
نشانی نشریه: www.jme.shahroodut.ac.ir
دانشگاه صنعتی شاهرود

بررسی مکانیسم جذب سولفات از پساب اسیدی معدنی بر روی گل قرمز و روش اصلاح آب دریا: مطالعات آزمایشگاهی و شبیه‌سازی مولکولی

شیما رحیمی* و مهدی ایران نژاد

بخش مهندسی معدن، دانشگاه صنعتی امیر کبیر، تهران، ایران

اطلاعات مقاله

تاریخ ارسال: ۲۰۲۵/۰۴/۱۴
تاریخ داوری: ۲۰۲۵/۰۵/۱۴
تاریخ پذیرش: ۲۰۲۵/۰۶/۰۹

DOI: 10.22044/jme.2025.16215.3137

کلمات کلیدی

مدلسازی فرکتالی
غلظت-فاصله از گسل
غلظت-حجم
تعداد-اندازه، نفوذپذیری

چکیده

در این مطالعه، گل قرمز (RM) به عنوان یک محصول جانبی در فرآیند تولید آلومینا از بوکسیت به عنوان جاذب برای جذب آلاینده سولفات از پساب اسیدی معدنی (AMD) استفاده شده است. رهاسازی AMD منجر به اسیدی شدن آبها می‌شود، که اثرات زیان باری برروی حیات آبزیان و سلامت انسان خواهد داشت. روش‌های خواص‌سنجی، مطالعات آزمایشگاهی و شبیه‌سازی‌های مولکولی برای بررسی جذب سولفات برروی RM انجام شدند. محاسبات ترمودینامیکی پس از بهینه‌سازی اکسیدهای فلزی موجود در ساختار گل قرمز با نرم‌افزار متریال استدیو و با استفاده از روش dmol3 و DFT انجام شدند. نتایج محاسبات انرژی جذب توسط ماژول مکان‌یاب جذب، انرژی جذب را به ترتیب برای Fe_2O_3، Al_2O_3، $CaCO_3$، TiO_2 و SiO_2، ۸۱۹/۰۹-، ۵۶۱/۷-، ۲۶۸/۸-، ۱۰۵/۴- و ۳۱۴/۷- کیلوکالری بر مول تعیین کرد. فعال‌ترین ترکیبات در ساختار گل قرمز (اکسیدهای آهن و آلومینیوم) هستند که به ترتیب ۲۲/۵٪ و ۱۳/۳٪ را در ساختار گل قرمز تشکیل می‌دهند. علاوه بر این، از شستشوی آب دریا به عنوان روش اصلاح گل قرمز استفاده شد که می‌تواند pH بالای آنرا کاهش داده و ظرفیت جذب گل قرمز خام را بهبود بخشد. همچنین تأثیر این روش اصلاح سطح با شبیه‌سازی حلال در محیط جذب سولفات برروی گل قرمز و با انتخاب ثابت دی‌الکتریک بررسی شد. برای آب به عنوان حلال اصلی با ثابت دی‌الکتریک ۷۸/۵۴، انرژی جذب RM برابر با ۳۵/۶۸- کیلوکالری بر مول محاسبه شد و برای محیط آب دریا با ثابت دی‌الکتریک ۸۶ به ۵۶/۶۹ -کیلوکالری بر مول افزایش یافت. بنابراین، RM می‌تواند به دلیل ارزان بودن و pH قلیایی که می‌تواند منجر به خنثی‌سازی AMD شود، به عنوان یک جاذب بالقوه سولفات در نظر گرفته شود.

نویسنده مسئول مکاتبات: sh.rahimi1983@yahoo.com (ش. رحیمی)